Acta Physiologica Sinica, April 25, 2012, 64(2): 107–120
http://www.actaps.com.cn

Research Paper

Mechanical properties and composition of mesenteric small arteries of simulated microgravity rats with and without daily $-G_x$ gravitation

GAO Fang[1,**], CHENG Jiu-Hua[1,**], BAI Yun-Gang[1], Marco Boscolo[3,△], HUANG Xiao-Feng[2], ZHANG Xiang[3], ZHANG Li-Fan[1,*]

[1]Department of Aerospace Physiology and Key Laboratory of Aerospace Medicine of Ministry of Education; [2]Central Laboratory, School of Basic Medical Sciences, the Fourth Military Medical University, Xi'an 710032, China; [3]Department of Aerospace Engineering, Cranfield University, Cranfield, MK 43 0AL, UK

Abstract: The aim of the present study was to evaluate the active and passive mechanical properties and wall collagen and elastin contents of mesenteric small arteries (MSAs) isolated from rats of 28-day simulated microgravity (SUS), countermeasure [S + D: SUS plus 1 h/d $-G_x$ to simulate intermittent artificial gravity (IAG)] and control (CON) groups. Three mechanical parameters were calculated: the overall stiffness (β), circumferential stress (σ_θ)-strain (ε_θ) relationship and pressure-dependent incremental elastic modulus ($E_{inc,p}$). Vessel wall collagen and elastin percentage were quantified by electron microscopy. The results demonstrate that the active mechanical behavior of MSAs differs noticeably among the three groups: the active stress-strain curve of SUS vessels is very close to the passive curve, whereas the active σ_θ-ε_θ curves of CON and S + D vessels are shifted leftward and display a parabolic shape, indicating that for MSAs isolated from S + D, but not those from SUS rats, the pressure-induced myogenic constriction can effectively stiffen the vessel wall as the CON vessels. The passive mechanical behavior of MSAs does not show significant differences among the three groups. However, the percentage of collagen is decreased in the wall of SUS and S + D compared with CON vessels in the following order: SUS < S + D < CON. Thus, the relationship between passive mechanical behavior and compositional changes may be complex and yet depends on factors other than the quantity of collagen and elastin. These findings have provided biomechanical data for the understanding of the mechanism of postflight orthostatic intolerance and its gravity-based countermeasure.

Key words: myogenic tone and reactivity; vascular remodeling; postflight cardiovascular deconditioning; intermittent artificial gravity

模拟失重大鼠肠系膜小动脉的力学特性与重塑变化及重力性对抗措施的防护效果

高 放[1,**]，程九华[1,**]，白云刚[1]，Marco Boscolo[3,△]，黄晓峰[2]，张 向[3]，张立藩[1,*]

第四军医大学[1]航空航天生理学教研室及教育部航空航天医学重点实验室；[2]中心实验室，西安 710032；[3]克兰菲尔德大学航空工程系，克兰菲尔德，MK43 0AL 英国

摘 要：为进一步阐明中期模拟失重环境下，肠系膜阻力性小血管的适应性改变及重力性对抗措施的防护效果，本文对28 d模拟失重组(SUS)、对抗措施组(S + D：每日使动物恢复正常站立体位1 h，承受$-G_x$方向的重力作用；其余23 h仍处于模拟失重状态)，以及对照组(CON)大鼠肠系膜第三级小动脉的生物力学特性与血管壁重塑变化进行了比较。所计算的生物力学参数包括：血管在被动状态下的表观刚度(β)；血管在主动和被动状态下的周向应力(σ_θ)-应变(ε_θ)关系及其增量弹性模量($E_{inc,p}$)。血管壁胶原和弹性蛋白的数量则以其在高倍透射电镜下截面积所占的百分比定量。结果显示，SUS组的主动σ_θ-ε_θ曲线非常靠近血管的被动曲线，表明其肌源性紧张度调节功能已基本丧失；但S + D的主动曲线则非常靠近CON组，二者都远离被动曲

Received 2011-10-08 Accepted 2011-12-09

This work was supported by the National Natural Science Foundation of China (No. 30470649 and 31070839).

[**] These authors contributed equally to this work.

[△]Present address: School of Engineering and Mathematical Sciences, City University, London, EC1V 0HB, UK.

[*]Corresponding author. Tel: +86-29-84774802; Fax: +86-29-84774387; E-mail: zhanglf@fmmu.edu.cn

线，明显左移，并呈抛物线状。S + D组的主动曲线反映跨壁压升高时，血管刚度主动增大使应变降低的过程；但重力性对抗措施似仍不能使其与CON组的血管完全相当。三组血管的被动生物力学特性未见有显著性差别：三组的β均值介于6.3~6.8；三组的被动σ_θ-ε_θ曲线及$E_{inc,p}$随压力的变化皆呈指数型增长；上述被动态参数在三组间皆无显著性的差别。然而，三组血管胶原蛋白截面积的百分比却有显著性差别。电镜图像显示，CON与S + D组大鼠中膜平滑肌细胞间隙胶原的面积显然远大于SUS组。形态测量表明：与 CON相比，S + D与SUS组管壁中膜胶原蛋白的截面积分别减少了27%与46% ($P < 0.01$)；而S + D与SUS组间的差别也具有显著性意义($P < 0.05$)。以上结果表明，除胶原与弹性蛋白的数量与比例因素外，血管的被动生物力学特性还取决于其它一些因素。本文从生物力学角度进一步阐明了航天飞行后立位耐力不良以及重力性对抗措施的机理。

关键词：肌源性紧张度和反应性；血管重塑；飞行后心血管功能失调；间断性人工重力
中图分类号：R318.01

The impaired cardiovascular response to standing after return from space might be among the highest risks to the safety, well-being, and performance of astronauts [1–3]. In addition to hypovolemia, inability to adequately elevate the total peripheral resistance is one of the key mechanisms contributing to postflight orthostatic intolerance [1,2, 4–6]. The cause of the impairment of vascular function on returning to Earth's 1-G environment is apparently related to the adaptation of resistance vessels to altered wall stress due to loss of hydrostatic pressure gradients during microgravity exposure [3,7,8]. Therefore, gravity-based countermeasures like intermittent artificial gravity (IAG) by incorporating a short-arm centrifuge into the spacecraft, or exercise within lower body negative pressure (LBNP), have been suggested for future spaceflight [3, 5, 7, 9–12].

In order to investigate vascular adaptation to microgravity in detail, tail-suspended, head-down tilt rat model has been used by some authors [13] to analyze the specific contribution of various portions of the vasculature by a multi-level approach, from direct measurement on isolated large conduit arteries and small resistance arteries and arterioles, to perfusion studies of vascular beds, as well as studies on conscious rats [8, 14–16]. Given that in humans the decrements in splanchnic vascular conductance could account for one-third of the total peripheral vascular conductance [17] and in conscious, freely moving rats, the main sites of mesenteric vascular resistance are in the arcade small arteries [18], it is vital to elucidate the adaptation of small mesenteric arteries (MSAs) during microgravity exposure. However, to our best knowledge, relevant studies published during 2000 to 2008 were restricted to functional studies with discrepancies in their results [19–22]. On the basis of previous work, we have shown recently that 28-day simulated microgravity (SUS) induces vessel wall atrophy, depressed myogenic tone and reactivity, and reduced agonist-induced vasoreactivity in mesenteric third-order arterioles; furthermore, these structural and functional changes can be fully prevented by the countermeasure of daily restoring to normal standing posture (S + D), which mimics IAG [23]. To better understand the mechanical behavior of the MSAs of SUS rats and to evaluate the actual stiffness and performance of the MSAs of S + D rats in maintaining an adequate total peripheral resistance to meet the challenge of orthostasis, it is essential to quantify the active mechanical properties of MSAs in myogenically active state [24–26]. In addition, to better understand the stiffness of the vessel wall due to the remodeling of acellular matrix components, it is also essential to calculate the passive mechanical properties and the elastic modulus of the nonlinear material, since the stress-strain relationship is independent of the vessel geometry [24–27]. Furthermore, biomechanics also plays a fundamental role in better understanding the adaptation of vessels to microgravity, since altered local mechanical stress in the vessel wall due to the removal of gravity has been considered to be the primary initiating factor [3, 7, 8, 28] and the regulation of wall stress has been further considered as the drive for remodeling via tone [29–32].

To assess the mechanical properties of the MSAs, it requires the construction of pressure-diameter (p-d) relationships in the presence and absence of VSM myogenic activity and to transform them to the stress-strain relationships [24–26]. To facilitate a comparison with other mechanical property calculations for arteries, Hayashi's stiffness parameter β, derived from an exponential p-d relationship [27] and Hudetz's incremental elastic modulus, $E_{inc,p}$ [33] were also calculated. On the basis of the previous findings [26,27,32,34,35], we also reasoned that changes in passive mechanical properties of

the MSAs from SUS and S + D rats might be related to the vessel wall remodeling and hence the amount of collagen and elastin in the vessel wall was also examined by morphometry under electron microscopy.

The objectives of the present study were: (1) to determine whether the myogenic reactivity and active mechanical behavior of the MSAs are altered by a 28-day simulated microgravity and whether these changes can be prevented by the countermeasure of daily 1-h $-G_x$ gravitation, (2) to investigate whether simulated microgravity with and without countermeasure also induce differential changes in the passive mechanical properties of the MSAs isolated from SUS and S + D compared with that of control rats, and (3) to clarify whether these changes in passive stiffness are related to the quantity and ratio of collagen and elastin in the vessel wall.

1 MATERIALS AND METHODS

1.1 *Animal model and experimental design*

1.1.1 *Tail-suspended, head-down tilt rat model*

The technique of tail suspension[13] with modification from our laboratory has been described in detail previously[36]. Briefly, the rats were maintained in an about –30° head-down tilt position with their hind limbs unloaded to simulate cardiovascular effect of microgravity. The controls were housed in identical Plexiglas cages, except that the tail suspension device was removed. All animals received standard lab chow and water *ad libitum* and were caged individually in a room maintained at 23 °C on a 12:12-h light-dark cycle.

1.1.2 *Model of daily short-duration $-G_x$ gravitation*

Daily stationary ground support in rat's normal orthostatic posture, or standing (STD), for 1 h was adopted to simulate the countermeasure effect of IAG as previously described[37,38]. For daily short-duration STD, the suspended rat was released from suspension and then placed into a 50-cm-long, tube-like metallic mesh cage maintained in horizontal position for 1 h. The rat could move forward and backward, but it could not turn around. Food and water were provided *ad libitum* at the front end of the cage. The gravity vector was $-G_x$.

1.1.3 *Experimental design*

All protocols and procedures were reviewed and approved by the Animal Care and Use Committee of the Fourth Military Medical University. Two separate protocols were carried out.

In protocol 1, pressure-diameter relationships for MSAs in active and passive states to a stepwise increase of transmural pressure (TMP) from 4 to 175 mmHg were determined twice for each vessel segment in an arteriograph. And then the circumferential stress (σ_θ)-strain (ε_θ) relationship and the stiffness parameter β and elasticity in response to an increment in pressure, $E_{inc,p}$, were calculated. Male Sprague-Dawley rats weighing between 230 and 260 g were randomly assigned to three experimental groups (n =10 rats/group): control (CON), tail suspension (SUS), and daily suspension for 23 h plus standing for 1 h (S + D). During the 28-day period, daily STD intervention was conducted between 08:00 and 09:00.

In protocol 2, wall composition of the MSAs of SUS, S + D and CON rats was measured by electron microscopy and compared. The ultrathin longitudinal middlemost sections prepared in our previous study [23] for wall histo-morphometry were reused under a higher magnification to measure the percentage of collagen and elastin in the vessel wall.

1.2 *Pressure arteriography*

After 28 days of simulation, rats from protocol 1 were anesthetized with pentobarbital sodium (50 mg/kg, i.p.) and killed by exanguination via the abdominal aorta. A segment of small intestine with attached mesentery was excised, placed in a dissecting dish with cold physiological salt solution (PSS), and then a third-order (3A) arteriole was isolated from the mesentery and surrounding fat tissue. The isolated arteriolar segment was transferred to a vessel chamber containing PSS and was cannulated at both ends. Then the chamber was transferred to the stage of an inverted microscope coupled to a video camera, a video micrometer, and a data acquisition system (Pressure Myograph System P110, DMT, Denmark). The isolated arteriole was perfused under a pressure of 25 mmHg for 10 min to remove any blood or debris and check for leaks. Changing to no-flow condition, the axial length of the arteriolar segment was adjusted to its *in-vivo* length as previously described[23]. The intraluminal pressure was increased to 125 mmHg to further detect the leaks and to remove any buckle from the vessel by adjusting the axial length. The arteriole was then warmed slowly to 37 °C and allowed to equilibrate at 50 mmHg for 1 h. The superfusion PSS gassed with 21% O_2-5% CO_2-74% N_2 was replaced every 15 min during the equilibration period. After equilibration, the pressure was cycled three times between 25

and 125 mmHg to reduce mechanical hysteresis[39].

To assess myogenic reactivity, intraluminal pressure was increased from 4 to 175 mmHg by increments of 25 mmHg. Each step was maintained for 5–10 min to allow the vessel to reach a steady-state diameter. After the first series of pressure steps, the superfusion PSS was replaced and equilibrated for 15 min, and then the second series of pressure steps was repeated. Finally, a passive pressure-diameter relationship was obtained by incubating the arterial segment with Ca^{2+}-free PSS containing 2 mmol/L EGTA for 30 min and repeating the protocol for assessing active response to pressure change twice for each vessel.

The myogenic tone was calculated as:

$$\text{myogenic tone (\%)} = (d_{i,p} - d_{i,a})/\, d_{i,p} \times 100 \quad (1)$$

where $d_{i,p}$ is the internal diameter determined in Ca^{2+}-free PSS and $d_{i,a}$ is the active internal diameter at a particular intraluminal pressure.

1.3 *Biomechanical property calculations*

In this study, the rat MSA is considered to be a thick-walled cylindrical tube with orthotropic elasticity and the wall material is assumed to be incompressible, homogeneous, and globally nonlinear [24,25,33].

1.3.1 *Circumferential stress (σ_θ)-strain (ε_θ) relationship*

Because the thin wall assumption, i.e., the ratio of wall thickness to internal radius < 0.1, is not valid for these vessels, Laplace's equation was not adopted for an accurate calculation of wall stress. The parameter σ_θ was calculated at the internal and external radius using the equation derived by Timoshenko for a hollow cylinder submitted to uniform pressure[40].

$$\sigma_\theta(r) = \frac{r_i^2 p_i}{r_e^2 - r_i^2}\left(1 + \frac{r_e^2}{r^2}\right) \quad (2)$$

where r is the radius, r_i is the internal radius, r_e is the external radius, and p_i is the transmural pressure, respectively.

The circumferential strain (ε_θ) was calculated by the definition of strain at the internal and external radius using

$$\varepsilon_\theta(r) = \frac{r - r_0}{r_0} \quad (3)$$

where r_0 is the radius at zero pressure (actually p_i was set at 4 mmHg).

1.3.2 *Overall stiffness parameter (β)*

β was calculated for the passive vessels by a curve-fitting technique. The logarithmic transformation of the p-d data and linear regression to find β was performed using the following equation[27].

$$\ln\left(\frac{p_i}{p_s}\right) = \beta\left(\frac{d_e}{d_s} - 1\right) \quad (4)$$

where p_i is the internal pressure, p_s is a reference pressure chosen in the physiological range, d_e is the external diameter, and d_s is the external diameter at the reference pressure. A reference pressure of 75 mmHg was chosen because it lies within the physiological pressure range and gave a good fit to the data (mean $R^2 > 0.90$).

1.3.3 *Incremental elastic modulus ($E_{inc,p}$)*

To determine the inherent wall elastic properties, $E_{inc,p}$ developed by Hudetz for orthotropic, incompressible arteries was calculated using the following equation[33].

$$E_{inc,p} = \frac{\Delta p}{\Delta r_i}\frac{2 r_i r_e^2}{r_e^2 - r_i^2} + \frac{2 p r_e^2}{r_e^2 - r_i^2} \quad (5)$$

where Δp is the incremental change in transmural pressure, Δr_i is the corresponding change in internal radius, and r_i, r_e, and p are the internal radius, external radius, and pressure at the beginning of the increment, respectively.

1.4 *Determination of wall composition*

Ultrathin sections of the same vessels used for electron microscopic measurements of cellular components in our previous study [23] were re-used for the measurements of acellular components at higher magnifications as previously described by Intengan *et al*. [41]. Briefly, the ultrathin longitudinal middlemost sections (70 nm) stained with 1% uranyl acetate and 1% lead citrate were examined with a JEM-2000EX transmission electron microscope (JEOL, Tokyo, Japan). Electron micrographs were taken at an original magnification of ×4 000 and enlarged by a factor of 3.75 for a final magnification of ×15 000. The areas of media (M) and adventitia (A) were measured and calculated, and then the areas occupied by collagen and elastin fibrils in M and A were measured by repeated tracing the edges of the profiles of these acellular components sectioned along different orientations in the electron micrographs by an image analysis software (Image-Pro Plus 6.0). Then the percentage of collagen and elastin in M and A were calculated. To insure uniform sampling, the quantification of the percentage of collagen and elastin was made randomly for a total of 4 or 5 non-overlapping micrographs from each vessel by two observers independently. The area of each micrograph measured was ~16 μm^2.

1.5 *Statistical analysis*

Values are means ± SEM. One vessel per rat was used for analyses. Model fits were considered highly correlated for $R^2 > 0.90$. A two-way ANOVA with repeated measures was used to determine the overall differences of the p-d relationship and passive $E_{inc,p}$ among the three groups and different intraluminal pressures of the same group and then the Student-Newman-Keuls *post hoc* test was used to determine the significance of differences among means. A one-way ANOVA was used to compare β values among the three groups. Comparisons of body weight and soleus wet weight, and myogenic tone (%) and dimensions of vessel segments at 100 mmHg were analyzed by Student's *t*-test. $P < 0.05$ was considered statistically significant. Statistical analysis was performed with the SPSS 9.0 package.

2 RESULTS

2.1 Body weight and soleus wet weight

The data are summarized in Table 1. There were no significant differences in final body weight among the three groups of protocol 1. The wet weight of soleus of SUS rats was 58% less than CON rats ($P < 0.01$). However, the soleus wet weight of S + D rats was 35% less than CON rats ($P < 0.01$), indicating the countermeasure effectiveness of 1-h/day STD in attenuating muscle atrophy[12, 38].

2.2 Vascular mechanics

2.2.1 Vessel characteristics

As shown in Table 2, in the first series, the passive external diameter ($d_{e,p}$) and lumen diameter ($d_{i,p}$) determined at 100 mmHg showed no significant differences among the three groups. However, the passive wall thickness (w_p) of MSAs from SUS was significantly less than CON and S + D rats ($P < 0.05$). The active external diameter ($d_{e,a}$) and lumen diameter ($d_{i,a}$) at 100 mmHg were significantly less in MSAs from CON and S + D than SUS rats ($P < 0.01$ or 0.05). And hence the myogenic tone at 100 mmHg was significantly greater ($P < 0.01$ or 0.05) in CON and S + D than SUS groups. The active wall thickness (w_a) was also significantly greater ($P < 0.05$) in CON than SUS vessels.

2.2.2 Pressure-diameter relationship

Figure 1*A* and *B* shows the pressure (p) *vs* external diameter (d_e) relationship of MSAs of the three groups under passive and active conditions during the first and second series of pressure steps. In passive state, the p-d_e relationship of the three groups displayed an exponential curve in the pressure range of 4–175 mmHg: diameter increased rapidly at lower pressures and slowly at higher pressures. These passive relationships were not significantly different among the three groups and the passive p-d_e curves of each group in the two series were also quite similar. In active state, external diameters of MSAs of the three groups were noticeably smaller than passive diameters due to SMC activation. For each group, the active p-d_e curves were also quite similar between the two series. However, the active p-d_e relationships did not fit an exponential relationship and displayed irregularly shaped curves that differ among the three groups, reflecting differences in myogenic tone and reactivity. In both the two series, all the active p-d_e curves shifted leftward from the passive curves and the extent of shift being greater in CON and S + D compared with SUS vessels. Between 50 and 150 mmHg, the CON and S + D maintained, respectively, a smaller and essentially constant diameter compared with that of SUS vessels. Whereas the p-d_e curve of the SUS vessels was situated close to the passive curves and displayed a nearly monotonic increase of diameter with increasing pressure. The differences between CON and SUS vessels reached the level of significance (1st series, $P < 0.01$; 2nd series, $P < 0.05$).

2.2.3 Active circumferential stress-strain relationship

The active σ_θ-ε_θ relationship did not fit an exponential relationship and behaved much differently among the three groups. The shape of active σ_θ-ε_θ curves for each group was quite similar between the two series, but all curves in the second series shifted rightward, indicating

Table 1. Body weight and wet weight of left soleus of CON, SUS and S + D rats in protocol 1

	Body weight (g)		Wet weight of left soleus	
	Initial	Final	Absolute (mg)	Relative (mg/g body weight)
CON	321.4 ± 9.2	445.7 ± 10.0	168.0 ± 4.9	0.38 ± 0.01
SUS	325.2 ± 10.9	432.5 ± 10.3	70.0 ± 5.6**	0.16 ± 0.01**
S + D	319.9 ± 9.6	437.6 ± 8.3	109.0 ± 4.3** ##	0.25 ± 0.01** ##

Values are means ± SEM, $n = 10$ animals/group. CON, control; SUS, 4-week tail-suspended; S + D, 23 h/d suspension + 1 h/d standing. **$P < 0.01$ *vs* CON; ##$P < 0.01$ *vs* SUS.

Table 2. Dimensions of segments of mesenteric third-order small arteries isolated from CON, SUS and S + D rats

	Vessel data at 100 mmHg			Group comparison		
	CON	SUS	S + D	CON *vs* SUS	SUS *vs* S + D	CON *vs* S + D
			First series (n = 10)			
$d_{e,p}$ (μm)	240.4 ± 9.4	247.4 ± 10.9	253.1 ± 7.5	NS	NS	NS
$d_{e,a}$ (μm)	167.8 ± 6.3	223.7 ± 12.7	195.1 ± 8.4	**	NS	*
$d_{i,p}$ (μm)	219.3 ± 9.6	228.0 ± 10.8	231.0 ± 8.0	NS	NS	NS
$d_{i,a}$ (μm)	141.8 ± 5.8	204.1 ± 12.9	173.1 ± 8.7	**	NS	**
w_p (μm)	10.8 ± 0.5	9.7 ± 0.3	11.1 ± 0.5	*	*	NS
w_a (μm)	13.0 ± 1.0	9.8 ± 0.7	11.0 ± 0.7	*	NS	NS
Tone (%)	34.5 ± 3.1	10.9 ± 2.6	24.2± 4.6	**	*	NS
			Second series (n = 10)			
$d_{e,p}$ (μm)	240.8 ± 9.9	249.3 ± 10.6	256.2 ± 8.2	NS	NS	NS
$d_{e,a}$ (μm)	180.2 ± 8.6	225.2 ± 15.3	211.0 ± 11.7	*	NS	NS
$d_{i,p}$ (μm)	218.1 ± 10.1	226.7 ± 10.4	231.3 ± 8.6	NS	NS	NS
$d_{i,a}$ (μm)	157.4 ± 8.7	205.8 ± 15.4	190.4 ± 11.8	*	NS	*
w_p (μm)	11.3 ± 0.6	11.3 ± 0.3	12.5 ± 0.7	NS	NS	NS
w_a (μm)	11.4 ± 0.7	9.7 ± 0.5	10.3 ± 0.6	NS	NS	NS
Tone, %	26.9 ± 4.6	10.0 ± 3.6	17.2 ± 4.7	**	NS	NS

Measurements were made on cannulated vessels pressurized to 100 mmHg. n = number of animals/group. d_e: external diameter; d_i: internal (lumen) diameter, w: wall thickness. Subscripts p and a represent passive and active state, respectively; NS means "not significant". $^*P < 0.05$, $^{**}P < 0.01$.

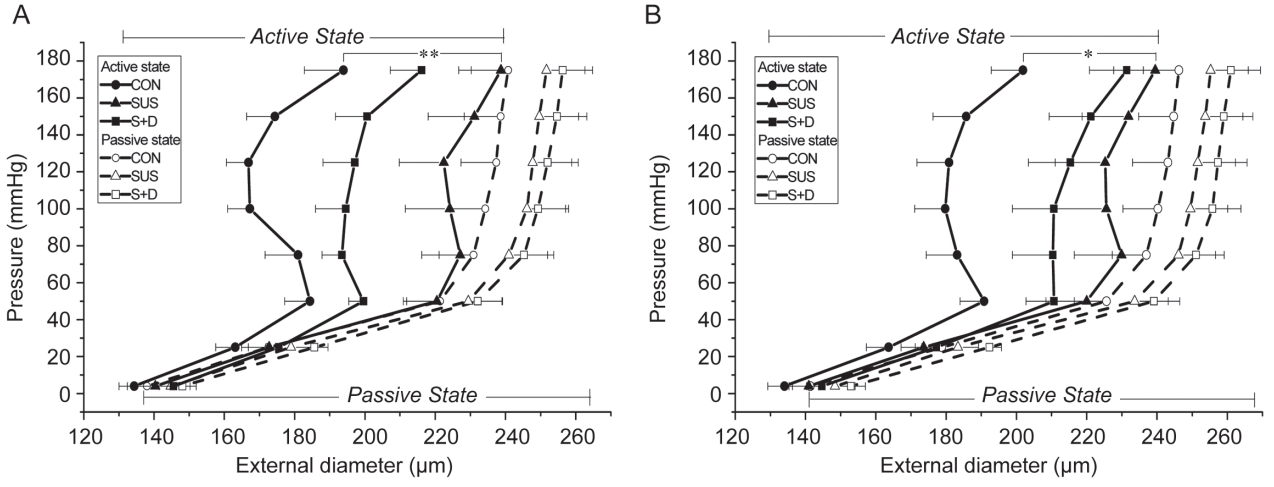

Fig. 1. Pressure-external diameter relationship of mesenteric third-order small arteries isolated from control (CON), 4-week suspended (SUS), and 23 h/d suspended + 1 h/d standing (S + D) rats in active and passive states within the intraluminal pressure range of 4–175 mmHg. Two separate series of pressure steps were performed. Data from the first and second series are depicted in *A* and *B*, respectively. Values are means ± SEM. In the first and second series, n= 10 per group. $^*P < 0.05$, $^{**}P < 0.01$ (2-way ANOVA).

an overall increase in strains to the second series of pressure steps. However, the extent of shift was greater in CON and S + D compared with SUS vessels; whereas σ_θ being kept at 1.25 (10^6 dyn/cm^2), ε_θ for the CON and S + D in the second series was increased by 30%, but for SUS the strain was increased by only 2% (Fig. 2*A* and *B*). In both series, the active σ_θ-ε_θ curves of CON and S + D vessels were situated leftward: below 50 mmHg, they were distensible at small strains; between 50 and 150 mmHg, a decrease in strain due to SMC activation generated an almost parabolic σ_θ-ε_θ curve within the myogenic pressure range; even at 175 mmHg, the active circumferential stress and strain of CON and S + D were still kept at a lower level com-

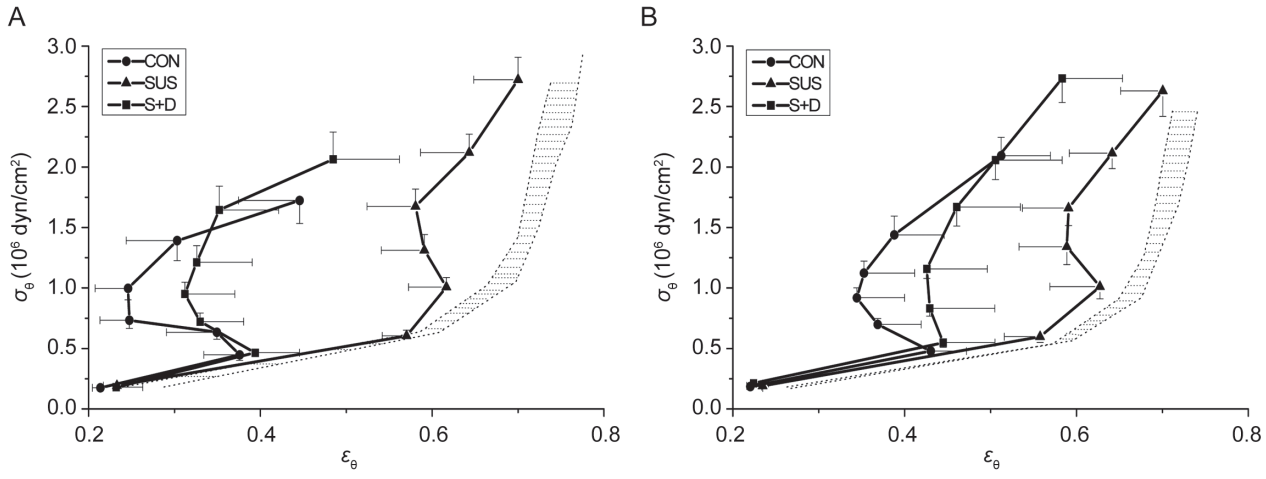

Fig. 2. Active stress (σ_θ)-strain (ε_θ) relationship of mesenteric third-order small arteries isolated from CON, SUS and S+D rats. Circumferential stress (σ_θ)) and strain (ε_θ) are both calculated at the internal radius. The relationships calculated from the data of the first and second series are depicted in *A* and *B*, respectively. Curves depicted in dotted lines situated at the right side of these active curves represent the position of respective passive stress-strain curves (see Fig.3). Values are means ± SEM. n = 10 per group.

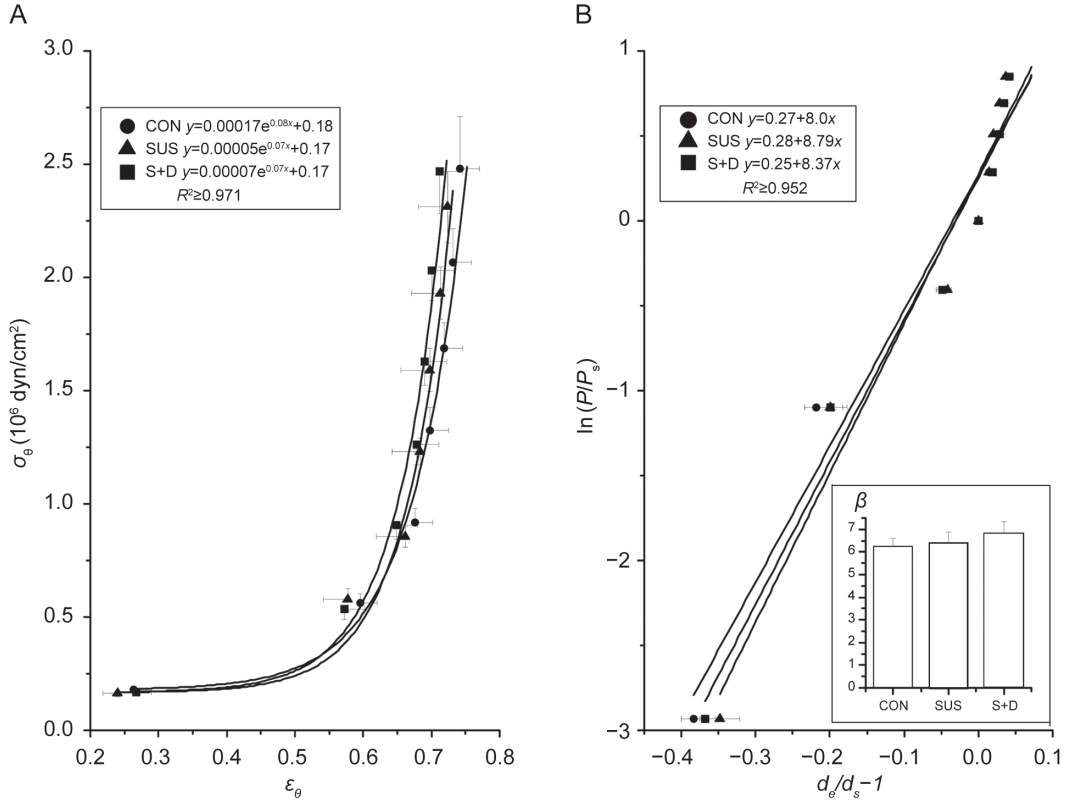

Fig. 3. Comparison on passive mechanical behavior of mesenteric third-order small arteries among CON, SUS and S + D groups. *A*: Circumferential stress (σ_θ)-strain (ε_θ) relationship for passive vessels calculated from the data of the second series. Circumferential σ_θ and ε_θ are both calculated at the external radius. Fitted curves are also shown with corresponding exponential equations and R^2 values. *B*: A representative linear regression between the logarithmic pressure ratio versus the distension ratio with β determined being shown in the bottom right inset. The calculation was based on the data from the second series. The reference pressure (P_s) was 75 mmHg. Values are means ± SEM. n = 10 per group.

pared with SUS vessels. Although the curves of CON and S + D vessels were close to each other, the leftward concavity was apparently more pronounced in CON than S + D vessels. By contrast, the active σ_θ-ε_θ curves of SUS vessels were situated rightward and close to the passive curves due to a higher distensibility at smaller strains and an attenuated myogenic activity at higher strains.

2.2.4 Passive mechanical property

Since the passive p-d_e relationships for the two series of each group were quite similar, so the passive σ_θ-ε_θ relationship and β value were only calculated based on the data of the second series. The passive vessels of the three groups exhibited a typical exponential σ_θ-ε_θ curve with increasing stiffness at higher strains and there were no significant differences among the three groups (Fig. 3*A*). The regression used to calculate β with the findings were shown in Fig. 3*B*. The average β values for CON, SUS and S + D groups were 6.3 ± 0.3, 6.4 ± 0.5 and 6.8 ± 0.5, respectively, and there were no significant differences in β values among the three groups (Fig. 3*B*, inset).

2.2.5 Incremental elastic modulus ($E_{inc,p}$)

$E_{inc,p}$ increased significantly with pressure for all passive vessels ($P < 0.05$) but it did not show significant differences among the three groups (Fig. 4*A*). In contrast, $E_{inc,p}$ for all active vessels remained relatively constant after each pressure increment, therefore, it is apparent that the passive $E_{inc,p}$ at higher pressures was noticeably higher than the modulus for active vessels (Fig. 4*B*). This was further confirmed by the highly significant differences between the passive and active values at 175 mmHg ($P < 0.01$).

2.3 Composition

Representative transmission electron-microscopic images of the middlemost longitudinal sections of MSAs from the three groups were shown in Fig. 5. The major components, i.e. endothelium, smooth muscle cell (SMC), internal elastic lamina (IEL), elastin and collagen, were clearly visible and the composition of MSAs was qualitatively similar among the three groups. The distribution and details of collagen (closed arrows) and elastin (open arrows) were shown in Fig. 5. Based on striation pattern and diameter, mainly type III collagen were observed between SMCs. Densely packed bundles of type I collagen were observed in the adventitia. Elastic fibers observed in M and A was mainly amorphous substance with varying electron-density surrounded by microfibrils at their periphery. The details of the images of collagen and elastin were further shown in the relevant insets. Most of the collagen fibrils were found in the adventitia (A) and a small amount was between SMCs in the media (M). As was shown in Fig. 5, in the intercellular spaces of the media, the areas of collagen were apparently greater in CON and S + D compared with CON vessel. Table 3 summarizes the morphometric data for collagen and elastin. The percentage of collagen in the vessel wall was 33%, being comparable

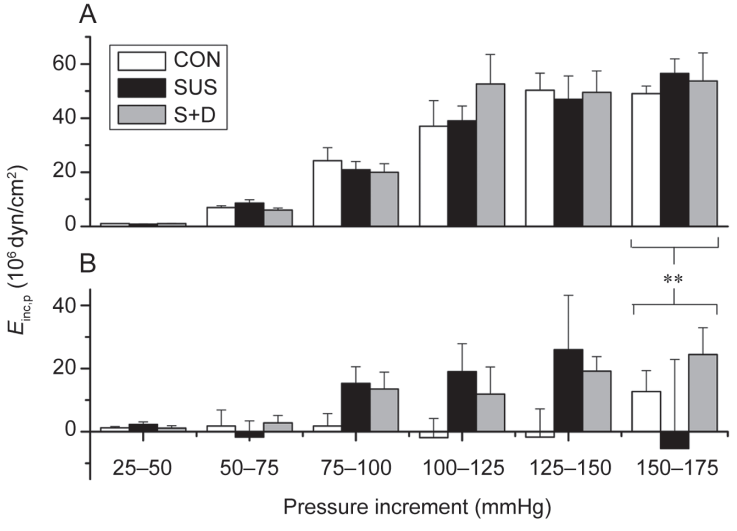

Fig. 4. Incremental elastic modulus ($E_{inc,p}$) of mesenteric third-order small arteries isolated from CON, SUS and S + D rats in passive (*A*) and active (*B*) states at six pressure increments. The increase in $E_{inc,p}$ in passive state over the six pressures was highly significant. The calculation was based on the data from the second series. Values are means ± SEM. $n = 10$ per group. $^{**}P < 0.01$.

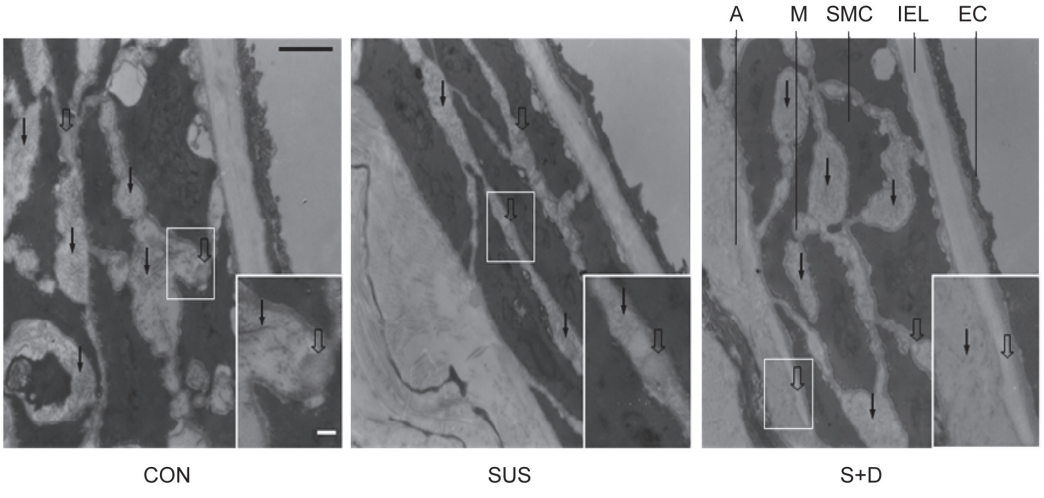

Fig. 5. Transmission electron micrographs of the longitudinal middlemost sections of the wall of mesenteric third-order small arteries from CON, SUS and S+D rats. Vessel specimens were prefixed in passive state at their *in-vivo* length under 75 mmHg for 60 min. Acellular matrix components, collagen (closed arrows) and elastin (open arrows) are clearly visible and their details are further shown in each relevant inset. Vessel histology, with regions of internal elastic lamina (IEL), media (M), and adventitia (A), and endothelial cell (EC) and smooth muscle cell (SMC) are also clearly shown. Scale bar, 500 nm. Electron micrographs in each inset, scale bar, 50 nm.

Table 3. IEL thickness and percentage of collagen and elastin in the wall of mesenteric small arteries of CON, SUS and S + D rats

	Mesenteric small artery		
	CON (n = 5)	SUS (n = 6)	S + D (n = 6)
IEL thickness (μm)	0.44 ± 0.02	0.26 ± 0.01**	0.30 ± 0.01$^{**\#\#}$
C_M (%)	17.7 ± 0.9	9.6 ± 1.1**	12.9 ± 1.3$^{**\#}$
C_A (%)	59. 2 ± 3.5	45.6 ± 3.4*	54.3 ± 2.5$^{\#}$
C_W (%)	33.1 ± 2.5	25.9 ± 2.1*	27.7 ± 1.9
E_M (%)	1.1 ± 0.2	1.0 ± 0.1	1.2 ± 0.1
E_A (%)	3.6 ± 0.7	3.1 ± 0.4	3.9 ± 0.4
E_W (%)	2.0 ± 0.2	1.9 ± 0.2	2.1 ± 0.2
$(E/C)_M$	0.065 ± 0.009	0.258 ± 0.107*	0.116 ± 0.018$^{*\#}$
$(E/C)_A$	0.063 ± 0.016	0.082 ± 0.017	0.072 ± 0.008
$(E/C)_W$	0.056 ± 0.006	0.093 ± 0.019*	0.079 ± 0.006*

Values are means ± SEM. CON, control group; SUS, tail-suspension group; S + D, 23 h/d suspension + 1 h/d standing. IEL, internal elastic lamina; C_M, C_A and C_W are percentages of collagen in the media, adventitia and wall, respectively; E_M, E_A and E_W are percentages of elastin in the media, adventitia and wall, respectively; $(E/C)_M$, $(E/C)_A$, and $(E/C)_W$ are ratios of elastin to collagen in the media, adventitia and wall, respectively. $^{*}P < 0.05$, $^{**}P < 0.01$ *vs* CON; $^{\#}P < 0.05$, $^{\#\#}P < 0.01$ *vs* SUS.

with the data of 31% reported by VanBavel *et al*.[42]. Comparing with CON, the percentage of collagen in A and M of SUS vessels decreased by 23% and 46% respectively ($P < 0.01$ or 0.05); whereas for S + D vessels, the percentage of collagen in M decreased by 27% ($P < 0.01$). Furthermore, the percentages of collagen in A and M of SUS were also significantly less than S + D vessels ($P < 0.05$). Elastin was confined primarily to the IEL. The thickness of IEL was significantly reduced ($P < 0.01$) in the following order: SUS < S + D < CON. Small amount of elastin was also observed in the MSAs' wall from the three groups. The percentage of elastin in A of SUS tended to be less compared with CON and S + D vessels, but the differences did not reach the level of significance.

3 DISCUSSION

The key findings are as follows: (1) The active mechanical behavior of MSAs differs noticeably among

the three groups: the active σ_θ-ε_θ curve of SUS vessel is very close to the passive curves, whereas the active σ_θ-ε_θ curves of CON and S + D vessels are close to each other and both are shifted leftward far from the SUS and display almost like a vertical line but with leftward concavity after an inflection point at a lower TMP. (2) The passive stress-strain relationship and the overall stiffness parameter β of MSAs do not show significant differences among the three groups, which is also supported by relevant passive $E_{inc,p}$ data. (3) The percentage of collagen is decreased in the wall of SUS and S + D compared with CON vessels in the following order: SUS < S + D < CON.

3.1 Active mechanical behavior

In order to evaluate fully the performance of myogenic mechanism of the isolated MSAs, three specific measures were taken in the experimental design. First, the experiment was designed to study the myogenic reactivity exclusively avoiding any agonist- or KCl-induced constrictions. Second, a very strict increasing pressure schedule ranging from 4 to 175 mmHg repeated twice for each vessel was adopted to challenge the myogenic mechanism. Third, the circumferential stress (σ_θ) was calculated using the Timoshenko's equation[40], since the thin-wall assumption required for the Laplace's equation is not valid for these vessels[24]. Similar consideration has also been noted in the work of Hayashi *et al*.[27].

According to Osol *et al*.[43], myogenic responses of small cerebral arteries may be partitioned into three distinct phases characterized by distinct changes in cytosolic calcium: (1) myogenic tone development, 40–60 mmHg (MT), (2) myogenic reactivity to subsequent pressure changes, 60–140 mmHg (MR), and (3) forced dilatation (FD) at >140 mmHg. The present study shows that in MSAs the myogenic response is relatively stable as evidenced by the close similarity of active p-d_e curves of the same group between the two series (Fig. 1*A* and *B*). At 100 mmHg, the differences in d_e for CON, S + D and SUS vessels between the two series were 12.5, 16.1 and 1.4 μm, respectively. Mechanisms that account for the different levels of susceptibility to this pressure schedule among the three groups remain to be elucidated.

The situation and shape of the active σ_θ-ε_θ curves reflect alterations in biomechanical behavior of SUS and S + D vessels compared with CON (Fig. 2). This also demonstrates why the constriction of deconditioned SUS vessels could not contribute importantly to maintain an adequate total peripheral resistance during orthostasis at 1 G. The situation and shape of SUS active σ_θ-ε_θ curve is close to and more like a passive curve, exhibiting a higher distensibility at small strains and a delayed and weak myogenic response to higher TMPs. By contrast, the active σ_θ-ε_θ curve of S + D is close to that of CON vessels and both are shifted leftwards and exhibit an almost parabolic shape, which demonstrates how the S + D can behave *in vivo* comparable to a CON vessel. The inflection of the curve at a small strain reflects a normal myogenic tone and the leftward concavity then in the curve indicates further stiffening of the vessels due to SMC activation within the normal myogenic pressure range which makes the vessels to experience smaller strains. Even at the highest pressure (175 mmHg), the stress and strain of CON and S + D still remain smaller than SUS vessel in the first series. Although it suggests that the countermeasure is effective in preventing the vessel deconditioning during simulated microgravity, the performance of S + D seems not to be comparable with normal CON vessels as indicated by an apparently smaller leftward concavity (1st and 2nd series) and the higher stress and strain values at 175 mmHg (2nd series) in S + D curves.

3.2 Passive mechanical behavior

In this study, three mechanical property measurements were used to quantify the passive mechanical behavior of the vessels and the results thus obtained are consistent in showing that the passive mechanical behavior of MSAs isolated from CON, SUS and S + D rats did not show significant change.

The passive vessels of the three groups exhibited a typical exponential stress-strain curve with increasing stiffness at higher strains (Fig. 3*A*). The shape of the passive curves is generally believed to depend on the contribution of elastin and collagen at low and high strains, respectively. Elastic fibers can easily be distended to around twice their resting length and collagen is a major nondistensible component in the arterial wall[24–26] and the "serial elements model" has been developed to explain the nonlinear passive curve of resistance vessels[32].

The overall stiffness parameter, β, has been used as a simple and reliable parameter for describing the passive p-d_e relationship in arteries[27]. Our average β value (6.3 ± 0.3) for MSAs of CON rats is lower than those found previously for rat cerebral resistance arteries,

such as 9.1 ± 1.1 [24] and 12.1 ± 1.1 (Zhang *et al*., unpublished data), which is also consistent with high β values of intracranial arteries in humans[27]. Although the dimensionless parameter β is useful, it does not necessarily reflect the inherent elastic properties of the wall material as it represents the apparent wall stiffness involving both the elastic modulus of the material and dimensions comprehensively.

Incremental elastic moduli (E_{inc}) are defined as elastic constants relating small changes in stress to small incremental strains at any initial state. Bergel [44] first applied it to express the elastic modulus of the nonlinear material like a vascular wall. In the present study, the equation for calculating $E_{inc,p}$ by Hudetz [33] was chosen, because it was developed to characterize incremental elastic properties of thick-walled, straight, cylindrically orthotropic, and incompressible arteries pressurized at a fixed length. The modulus $E_{inc,p}$ characterizes the radial and tangential stiffness complexly and has been used for small cerebral resistance arteries [27,28,45]. $E_{inc,p}$ was calculated for vessels at both active and passive states. The result indicates that the passive vessels were increasingly stiff as pressure increased (Fig. 4*A*), whereas the active vessels maintained relatively constant wall stiffness due to myogenic reactivity of SMCs (Fig. 4*B*).

3.3 Acellular matrix components

As the passive mechanical behavior of MSAs did not show significant differences among the three groups, the major acellular components may be expected to be of no significant change. However, morphometry by electron microscopy revealed that the opposite to be true: the percentage of collagen is decreased in the wall of SUS and S + D compared with CON vessel in the following order: SUS < S + D < CON; and the percentage of elastin in SUS also tended to be less than CON and S + D vessels (Table 3). The relationship of vascular structure and distensibility is complex and no doubt depends on factors other than proportional composition, including the distributions, orientations, and interconnections of the intramural constituents [26,32,34]. For example, the reduced distensibility of middle cerebral arteries from SHRSP compared with SHR was associated with a non-uniform distribution of the lessened collagen[35]. Further examples are from both animal and human studies: early in hypertension, the vessel wall components may be less stiff even though the collagen deposition is increased; but as hypertension progresses the wall stiffness may be normalized due to other changes, such as extracellular matrix-SMC anchoring; and later in advanced hypertension, the increased stiffness may develop (for review see: Intengan and Schiffrin 2001[34]). Therefore, elucidation of the long-term effect of SUS and S + D on vessel stiffness and its association with changes in collagen and elastin is warranted to evaluate the effectiveness of IAG.

3.4 Implications

Active mechanical property measurement reveals that after a medium-term simulated microgravity the deconditioned MSA behaves almost like a passive vessel, losing the ability to actively stiffen the vessel wall effectively. This could potentially be an underlying mechanism of postflight orthostatic intolerance in humans, because the decrements in splanchnic vascular conductance may account for one-third of the total peripheral vascular adjustment [17]. Another functional consequence could be a reduction of aerobic capacity and endurance [45]. In animal studies, it has been shown that following SUS the ability to redistribute cardiac output during exercise is impaired[46,47] and about 10% of the blood flowing to active muscles at exercise intensities eliciting maximal oxygen consumption is due to vasoconstriction in the splanchnic bed [49]. Active mechanical property evaluation further reveals the differences in active mechanical behavior between S + D and CON vessels, though our previous study has not identified any differences in function and structure between them [23]. In addition, the present study further shows that the reduction in percentage of collagen cannot be prevented by the countermeasure of daily 1-h $-G_x$ over 28 days. Therefore, the effectiveness of IAG in preventing vascular deconditioning during long-duration microgravity exposure should be further evaluated.

The concept that tone drives remodeling was quantitatively analyzed by Fridez *et al*.[29] for conduit artery and by Jacobsen *et al*.[30] and Van den Akker *et al*. [32] for small resistance artery. Both models highlighted the key role of myogenic tone in vascular adaptation to a sustained pressure increase: first by adjusting the degree of constriction and consequently the active stress during the initial phase; and then the vascular tone returns back to normal levels towards a restoration of baseline circumferential stress once the slower remodeling is developed sufficiently. These concepts seem also applicable to explain the tone-driven adaptation of MSAs to lowered TMPs during SUS. Lowered local TMPs in these resistance arteries during chronic head-

down tilt cause a reduction in tone and active wall stress and then remodeling, including wall atrophy[23] and a decrease of collagen percentage in the present study. Nevertheless, how to elucidate the underlying mechanism of the surprising effectiveness of IAG in preventing vascular adaptation[12,23,37] along the lines of these biomechanical, biophysical, and modeling approaches[29,30,32] remains a big challenge.

If such a tone-driven adaptation does occur in the small resistance arteries of splanchnic vascular bed of humans undergoing prolonged bed rest or spaceflight, these arterial adaptations might compromise the orthostatic tolerance and exercise capacity in 1-G environment. Recent work has suggested the possibility that needs further clarification. For example, Norsk and Christensen[49] reported that weightlessness in space for at least one week leads to a decrease in systemic vascular resistance. Based on the data from 26 cosmonauts flown 8 to 438 days, Kotovskaia and Fomina[50] reported that arterial resistance went down in essentially all vascular regions below the heart level. Furthermore, less arterial vasoconstriction in the legs and splanchnic circulation were associated with orthostatic intolerance after bed rest[51–53] and the countermeasure of exercise within LBNP may counteract orthostatic intolerance and reductions in aerobic capacity associated with bed rest (for review see: Hargens and Richardson 2009 [7]; Lee *et al*. 2010[45]). As has been shown in our previous study [54], the deconditioning effect on MSAs and its prevention by the countermeasure can be observed even after a 3-day simulation, suggesting that a rapid adaptation in myogenic mechanism is coming into action. However, judged from the degree of leftward shift of both active p-d and σ_θ-ε_θ curves of CON and S + D from that of SUS group, the "tone-driven adaptation" has become more conspicuous as vascular structural adaptation has fully developed after a medium-term simulation [23].

In conclusion, after a medium-term simulated microgravity the deconditioned MSA behaves almost like a passive vessel, losing the ability to actively stiffen the vessel wall, which can be effectively prevented by the countermeasure of 1 h/d $-G_x$. However, there are no significant differences in passive mechanical behavior of MSAs among the three groups, though the percentage of collagen is decreased in the wall of SUS and S + D compared with that of CON vessels, which suggests that the relationship between passive mechanical behavior and compositional changes further depends on factors other than proportional composition of collagen and elastin.

ACKNOWLEDGMENTS: We thank Professor XIA Jie-Lai for his advice in statistics analysis.

REFERENCES

1 Norsk P. Cardiovascular research in space. Respir Physiol Neurobiol 2009; 169: S2–S3.

2 Sides MB, Vernikos J, Convertino VA, Stepanek J, Tripp LD, Draeger J, Hargens AR, Kourtidou-Papadeli C, Pavy-LeTraon A, Russomano T, Wong JY, Buccello RR, Lee PH, Nangalia V, Saary MJ. The Bellagio report: cardiovascular risks of spaceflight: implications for the future of space travel. Aviat Space Environ Med 2005; 76: 877–895.

3 Watenpaugh DE, Hargens AR. The cardiovascular system in microgravity. In: Handbook of Physiology: Section 4: Environmental Physiology. Fregly B, Blatties CM, Fregly MJ, Ed. American Physiological Society, 1996, 631–674.

4 Buckey JC, Lane LD, Levine BD, Watenpaugh DE,Wright SJ, Moore WE, Gaffney FA, Blomqvist CG. Orthostatic intolerance after spaceflight. J Appl Physiol 1996; 81: 7–18.

5 Hargens AR, Watenpaugh DE. Cardiovascular adaptation to space-flight. Med Sci Sports Exerc 1996; 28: 977–982.

6 Meck JV, Reyes CJ, Perez SA, Goldberger AL, Ziegler MG. Marked exacerbation of orthostatic intolerance after long- vs. short-duration spaceflight in veteran astronauts. Psychosom Med 2001; 63: 865–873.

7 Hargens AR, Richardson S. Cardiovascular adaptations, fluid shifts, and countermeasures related to space flight. Respir Physiol Neurobiol 2009; 169: S30–S33.

8 Zhang LF. Vascular adaptation to microgravity: what have we learned? J Appl Physiol 2001; 91: 2415–2430.

9 Clement G, Pavy-Le Traon A. Centrifugation as a countermeasure during actual and simulated microgravity: a review. Eur J Appl Physiol 2004; 92: 235–248.

10 Vernikos J, Ludwig DA, Ertl A, Wade CE, Keil L, O'Hara DB. Effect of standing or walking on physiological changes induced by head down bed rest: implications for space flight. Aviat Space Environ Med 1996; 67: 1069–1079.

11 Vil-Viliams IF, Kotovskaya AR, Nikolashin GF, Lukjanuk VJ. Modern view on the short-arm centrifuge as a potential generator of artificial gravity in piloted missions. J Gravit Physiol 2001; 8: P145–P146.

12 Zhang LF. System specificity in responsiveness to intermittent $-G_x$ gravitation during simulated microgravity in rats. J Gravit Physiol 2005; 12: P1–P4.

13 Morey-Holton ER, Globus RK. Hindlimb unloading rodent model: technical aspects. J Appl Physiol 2002; 92: 1367–

1377.

14 Delp MD, Colleran PN, Wilkerson MK, McCurdy MR, Muller-Delp J. Structural and functional remodeling of skeletal muscle microvasculature is induced by simulated microgravity. Am J Physiol Heart Circ Physiol 2000; 278: H1866–H1873.

15 Delp MD, Holder-Binkley T, Laughlin MH, Hasser EM. Vasoconstrictor properties of rat aorta are diminished by hindlimb unweighting. J Appl Physiol 1993; 75: 2620–2628.

16 Zhang LF, Cheng JH, Liu X, Wang SY, Liu Y, Lu HB and Ma J. Cardiovascular changes of conscious rats after simulated microgravity with and without daily -G_x gravitation. J Appl Physiol 2008; 105: 1134–1145.

17 Rowell LB. Human Cardiovascular Control. New York: Oxford University Press, 1993, 1–80, 118–161.

18 Fenger-Gron J, Mulvany MJ, Christensen KL. Mesenteric blood pressure profile of conscious, freely moving rats. J Physiol 1995; 488.3: 753–760.

19 Behnke BJ, Zawieja DC, Gashev AA, Ray CA, Delp MD. Diminished mesenteric vaso- and venoconstriction and elevated plasma ANP and BNP with simulated microgravity. J Appl Physiol 2008; 104: 1273–1280.

20 Colleran PN, Behnke BJ, Wilkerson MK, Donato AJ, Delp MD. Simulated microgravity alters rat mesenteric artery vasoconstrictor dynamics through an intracellular Ca^{2+} release mechanism. Am J Physiol Regul Integr Comp Physiol 2008; 294: R1577–R1585.

21 Hatton DC, Yue Q, Chapman J, Xue H, Dierickx J, Roullet C, Coste S, Roullet JB, McCarron DA. Blood pressure and mesenteric resistance arterial function after spaceflight. J Appl Physiol 2002; 92: 13–17.

22 Looft-Wilson RC, Gisolfi CV. Rat small mesenteric artery function after hindlimb suspension. J Appl Physiol 2000; 88: 1199–1206.

23 Lin LJ, Gao F, Bai YG, Bao JX, Huang HF, Ma J, Zhang LF. Contrasting effects of simulated microgravity with and without daily –G_x gravitation on structure and function of cerebral and mesenteric small arteries in rats. J Appl Physiol 2009; 107: 1710–1721.

24 Coulson RJ, Chesler NC, Vitullo L, Cipolla MJ. Effects of ischemia and myogenic activity on active and passive mechanical properties of rat cerebral arteries. Am J Physiol Heart Circ Physiol 2002; 283: H2268–H2275.

25 Coulson RJ, Cipolla MJ, Vitullo L, Chesler NC. Mechanical properties of rat middle cerebral arteries with and without myogenic tone. J Biomech Eng 2004; 126: 76–81.

26 Humphrey JD. Cardiovascular Solid Mechanics: Cells, Tissues and Organs. New York; Springer-Verlag, 2001.

27 Hayashi K, Nagasawa S, Naruo Y, Okumura A, Moritake K, Handa H. Mechanical properties of human cerebral arteries. Biorheology 1980; 17: 211–218.

28 Gao F, Bao JX, Xue JH, Huang J, Huang WQ, Wu SX, Zhang LF. Regional specificity of adaptation change in large elastic arteries of simulated microgravity rats. Acta Physiol Hung 2009; 96: 167–187.

29 Fridez P, Rachev A, Meister JJ, Hayashi K, Stergiopulos N. Model of geometrical and smooth muscle tone adaptation of carotid artery subject to step change in pressure. Am J Physiol Heart Circ Physiol 2001; 280: H2752–H2760.

30 Jacobsen JC, Mulvany MJ, Holstein-Rathlou NH. A mechanism for arteriolar remodeling based on maintenance of smooth muscle cell activation. Am J Physiol Regul Integr Comp Physiol 2008; 294: R1379–R1389.

31 Prewitt RL, Rice DC, Dobrian AD. Adaptation of resistance arteries to increases in pressure. Microcirculation 2002; 9: 295–304.

32 Van den Akker J, Schoorl MJC, Bakker ENTP, vanBavel E. Small artery remodeling: current concepts and questions. J Vasc Res 2010; 47: 183–202.

33 Hudetz AG. Incremental elastic modulus for orthotropic incompressible arteries. J Biomech 1979; 12: 651–655.

34 Intengan HD, Schiffrin EL. Vascular remodeling in *H*ypertension: roles of apoptosis, inflammation, and fibrosis. Hypertension 2001; 38 (part 2): 581–587.

35 Izzard AS, Graham D, Burnham MP, Heerkens EH, Dominiczak AF, Heagerty AM. Myogenic and structural properties of cerebral arteries from the stroke-prone spontaneously hypertensive rat. Am J Physiol Heart Circ Physiol 2003; 285: H1489–H1494.

36 Zhang LN, Zhang LF, Ma J. Simulated microgravity enhances vasoconstrictor responsiveness of rat basilar artery. J Appl Physiol 2001; 90: 2296–2305.

37 Sun B, Zhang LF, Gao F, Ma XW, Zhang ML, Liu J, Zhang LN, Ma J. Daily short-period gravitation can prevent functional and structural changes in arteries of simulated microgravity rats. J Appl Physiol 2004; 97: 1022–1031.

38 Zhang LF, Sun B, Cao XS, Liu C, Yu ZB, Zhang LN, Cheng JH, Wu YH, Wu XY. Effectiveness of intermittent –G_x gravitation in preventing deconditioning due to simulated microgravity. J Appl Physiol 2003; 95: 207–218.

39 Osol G, Brekke JF, McElory-Yaggy K, Gokina NI. Myogenic tone, reactivity, and forced dialatation: a three-phase model of *in vitro* arterial myogenic behavior. Am J Physiol Heart Circ Physiol 2002; 283: H2260–H2267.

40 Timoshenko S. Theory of Elasticity. New York: McGraw-Hill, 1934.

41 Intengan HD, Deng LY, Li JS, Schiffrin EL. Mechanics and composition of human subcutaneous resistance arteries in essential hypertension. Hypertension 1999; 33 (1 Pt 2): 569–574.

42 VanBavel E, Siersma P, Spaan JA. Elasticity of passive blood vessels: a new concept. Am J Physiol Heart Circ Physiol 2003; 285: H1986–H2000.
43 Osol G, Halpern W. Myogenic properties of cerebral blood vessel from normotensive and hypertensive rats. Am J Physiol Heart Circ Physiol 1985; 249: H914–H921.
44 Bergel DH. The static elastic properties of the arterial wall. J Physiol 1961; 156: 445–457.
45 Lee SMC, Moore AD, Everett ME, Stenger MB, Platts SH. Aerobic Exercise deconditioning and contermeasures during bed rest. Aviat Space Environ Med 2010; 81: 52–63.
46 McDonald KS, Delp MD, Fitts RH. Effect of hindlimb unweighting on tissue blood flow in the rat. J Appl Physiol 1992; 72: 2210–2218.
47 Woodman CR, Sebastian LA, Tipton CM. Influence of simulated microgravity on cardiac output and blood flow distribution during exercise. J Appl Physiol 1995; 79: 1762–1768.
48 Armstrong RB, Delp MD, Goljan EF, Laughlin MH. Distribution of blood flow in muscles of miniature swine during exercise. J Appl Physiol 1987; 62: 1285–1298.
49 Norsk P, Christensen NJ. The paradox of systemic vasodilation and sympathetic nervous stimulation in space. Respir Physiol Neurobiol 2009; 169: S26–S29.
50 Kotovskaia AR, Fomina GA. The features of adaptation and disadaptation of the human cardiovascular system in the space flight conditions (in Russian). Fiziol Cheloveka 2010; 36: 78–86.
51 Arbeille P, Bernard S, Kerbeci P, Mohty DM. Portal vein cross-sectional area and flow and orthostatic tolerance: a 90-day bed rest study. J Appl Physiol 2005; 99: 1853–1857.
52 Arbeille P, Kerbeci P, Mattar L, Shoemaker JK, Hughson R. Insufficient flow reduction during LBNP in both splanchnic and lower limb areas is associated with orthostatic intolerance after bedrest. Am J Physiol Heart Circ Physiol 2008; 295: H1846–H1854.
53 Hughson RL. Recent findings in cardiovascular physiology with space travel. Respir Physiol Neurobiol 2009; 169: S38–S41.
54 Cheng JH (程九华), Boscolo M, Lin LJ, Bai YG, Zhang X, Ma J, Zhang LF. Comparison of biomechanical behavior of cerebral and mesenteric small arteries of simulated microgravity rats. Acta Physiol Sin (生理学报) 2009; 61(4): 386–394 (Chinese, English abstract).